Rheologica Acta
https://doi.org/10.1007/s00397-022-01331-6

REVIEW

Interactive Shear and Extensional Rheology—25 years of IRIS Software

Leslie Poh[1,2] · Esmaeil Narimissa[1,2] · Manfred H. Wagner[3] · H. Henning Winter[4]

Received: 9 September 2021 / Revised: 29 November 2021 / Accepted: 5 February 2022

Abstract

Over the past 25 years, IRIS has become an integral resource in materials laboratories around the world, bringing together stimulating communities of rheology experimentalists and theoreticians, rheological experts, and experts from other fields, and even making rheology accessible to non-rheologists. The calculational tools of IRIS interface data from different experimental findings with predictions from rheology theories. Since its beginning, many theory groups used IRIS to share their original codes for rheology predictions. We demonstrate this in two examples, (1) the detailed analysis of small amplitude oscillatory shear data (SAOS) and predictions thereof and (2) a theory, newly implemented in IRIS, that elegantly unites dynamical quantities from small amplitude oscillatory shear (SAOS) with data from filament stretching rheometry and predictions of transient shear. IRIS supports this convergence with a standardizing data (Dealy et al., J Rheol 39:253-265, 1995), which makes data sharing easy and independent of instrument brand-specific and laboratory-specific coding.

Keywords Data driven rheology · IRIS rheology software · High density polyethylene · Solution styrene–butadiene rubber · HMMSF model

Introduction

By 1996, the year when the Interactive Rheology Information System (IRIS) project took shape, rheology had sustained a prolonged period of stimulating growth. Advanced instrumentation and creative experimental techniques had generated reliable rheological data on a wide range of materials, which in turn led to innovative new materials and materials optimization and inspired theoretical work that successfully modeled the dynamics of viscoelastic materials. Well-established experimental tools and consolidated theories became available, but they maintain their own identity and remain separate from each other for the most part. Given all this progress, the obvious next challenge was to find a way to support the interaction between diverse rheological models and data. The interaction should be facilitated in an easy-to-use format so that diverse user communities could participate in such interaction and benefit from it, including academics, industry professionals, and even non-experts and newcomers to rheology. IRIS was developed to address this need for interaction and access.

The IRIS software interfaces experimental findings with predictions from rheological theories (as demonstrated by the examples shown further below). Results are presented quantitatively, with access to data tables, and also in visual form. And this applies not only to a single experiment or a single theory, but rather integrates as many diverse experiments and theories as needed for advancing an ongoing research project.

The interactive capabilities of IRIS have become possible through a platform architecture consisting of a central platform with satellite codes attached (Winter and Mours 2006). Repetitive user actions are assigned to the central platform which interfaces with a large number of satellite codes. Each satellite is dedicated to a specific experimental task or a specific rheology

✉ Leslie Poh
Leslie.Poh@gtiit.edu.cn

H. Henning Winter
winter@umass.edu

1 Department of Chemical Engineering, Technion–Israel Institute of Technology (IIT), Technion City, 32 000 Haifa, Israel

2 Department of Chemical Engineering, Guangdong Technion–Israel Institute of Technology (GTIIT), Shantou 515063, China

3 Polymer Engineering/Polymer Physics, Berlin Institute of Technology (TU Berlin), Ernst-Reuter-Platz 1, 10587 Berlin, Germany

4 Chemical Engineering and Polymer Science & Engineering, University of Massachusetts Amherst, 159 Goessmann Lab, Amherst, MA 01003-3110, USA

Published online: 16 March 2022

theory. More and more of these satellites have been created over the past 25 years. IRIS users can even create their own satellite code and interface it with all the others on the IRIS platform.

Scope of IRIS

Early satellite examples for the IRIS platform focused on experimental tasks such as:

- Time–temperature superposition (tTS) (Colby 1989; Ferry 1980) and also time-composition superposition of small amplitude oscillatory shear (SAOS) data as measured at a set of different temperatures and/or different compositions. Shifting merges the data into master curves based on their shift factors for time and composition level. Temperature shift factors are conveyed in terms of an intrinsic material temperature scale, E/R [K], and by providing parameter values for Arrhenius, Williams–Landel–Ferry (WLF) (Williams et al. 1955), and Vogel–Fulcher–Tammann–Hesse models (Dealy and Larson 2006; Williams, et al. 1955). The tTS analysis options in IRIS include the Kaelble inflection model of the non-diverging relaxation times near a glass transition. (Rowe and Sharrock 2011; Laukkanen and Winter 2018).
- Calculation of discrete and continuous relaxation time spectra, $H(\tau)$, by converting SAOS results from the frequency domain to the time domain (Baumgärtel and Winter 1989, 1992).
- Predicting creep behavior from SAOS,
- Time resolved SAOS (Mours and Winter 1994), including the respective mutation number values, of transient materials during cross-linking, during gelation, or during recovery from large amplitude shear (LAOS), etc.,
- Gelation analysis (Liu et al. 2017)
- Shifting of steady shear viscosity data and fitting them to empirical viscosity functions. (Carreau 1972; Yasuda et al. 1981),
- Analyzing transient viscosity data in shear or extension.

These are the main satellite codes and functions which have been used widely. Results get interfaced and communicated with an interactive plotting routine, which supports overlays, editing, and variable formats including Bowditch–Lissajous curves (Ewoldt et al. 2008). Besides plotting as usual, the interactive plots allow data export by digitization of the continuous or discrete functions in the plot. IRIS keeps backups of recently prepared plots, ready to be re-activated when needed again.

While the initial IRIS focused on the analysis and exploration of experiments, many theory satellites followed soon after. These theories seek to explain and predict the rheological behaviors of soft matter:

- Classical theories such as Rouse (1953), Zimm (1956), Maxwell (1867), Lodge Rubberlike Liquid (1956), and Doi-Edwards relaxation spectrum (Doi and Edwards 1978).
- Palierne theory for phase separated blends (Palierne and Lequeux 1991).
- Tube dilution theory of McLeish and coworkers (Blackwell et al. 2001; McLeish et al. 1999; McLeish and Larson 1998; Milner and McLeish 1997, 1998; Pryke, et al. 2002).
- Molecular stress function (MSF) model of Wagner and coworkers (Wagner et al. 2001, 2003).
- Hierarchical model of Larson and coworkers (Larson 2001; Park and Larson 2004, 2005).
- Mode coupling theory of Fuchs and Ballauff (Fuchs and Ballauff 2005a, 2005b; Fuchs and Cates 2002a, b; Voigtmann et al. 2004).
- Viscoelastic constitutive model of Phan-Thien and Tanner (1977).
- Molar mass prediction from SAOS (Cocchini and Nobile 2003; Nobile and Cocchini 2001).
- Introduction of molecular dynamics simulation (Masubuchi et al. 2003, 2004, 2001).
- Hierarchical multi-mode molecular stress function model (HMMSF) of Narimissa and Wagner (Narimissa et al. 2015, 2016; Narimissa and Wagner 2016c).

In addition, specific material groups are represented in IRIS with satellite codes (empirical models) such as the dual structural model for a linear superposition of two relaxation mechanisms (Stephens et al. 1988), the Winter–Chambon (WC) spectrum for gelation (Winter and Chambon 1986), the Baumgärtel–Schausberger–Winter (BSW) spectrum for long linear flexible polymers and for the glass transition (Baumgärtel et al. 1990), and the Yavitt–Winter (YW) spectrum for bottlebrush diblock co-polymers (Yavitt et al. 2019).

Several of the IRIS functions will be demonstrated in the next sections, starting with a *linear* viscoelastic analysis that results in a rich set of material functions. This is followed by an example of *nonlinear* viscoelastic analysis and modeling in the context of filament stretching. Linear viscoelastic and extensional data are scanned from a publication, entered into IRIS, and after having calculated the relaxation time spectrum from these data, elongational flow behaviors are predicted with the HMMSF model and overlaid with the experimental data that were scanned from the publication. Also, predictions of planar and biaxial extension as well as shear viscosity and first normal stress function are presented.

Example: Linear Viscoelastic Data Analysis and Modeling

A complex material expresses itself rheologically in a wide range of material functions. Many of these can be derived from a small amplitude oscillatory shear (SAOS) experiment. This is demonstrated here with dynamic moduli, G' and G'', of a solution styrene–butadiene rubber

from Synthos S.A. (Oswiecim, Poland) as measured in an Alpha RPA2000s using frequency scans at seven temperatures, Fig. 1a. Higher temperatures result in a lower G', which becomes more visible in the multi-frequency heating scan, Fig. 1b. Horizontal shifting combines the entire data set into master curves, here at a reference temperature of $T = 90$ °C, Fig. 1c. By applying time–temperature shift to this polymer, the experimental frequency window is significantly broadened. The horizontal shift factor, a_T, follows the well-known WLF format (Ferry 1980), Fig. 1d. The continuous spectrum, $H(\tau)$, Fig. 1e, calculated with the parsimonious model (Baumgärtel and Winter 1989, 1992), shows the positive power-law characteristic of a polymer near its glass transition (Winter 2013), which was an unexpected result of this analysis. Knowledge of $H(\tau)$ allows calculation of many material functions (Ferry 1980). Examples are the relaxation modulus $G(t)$ and the creep compliance $J(t)$, Figs. 1f and g. For linear polymers,

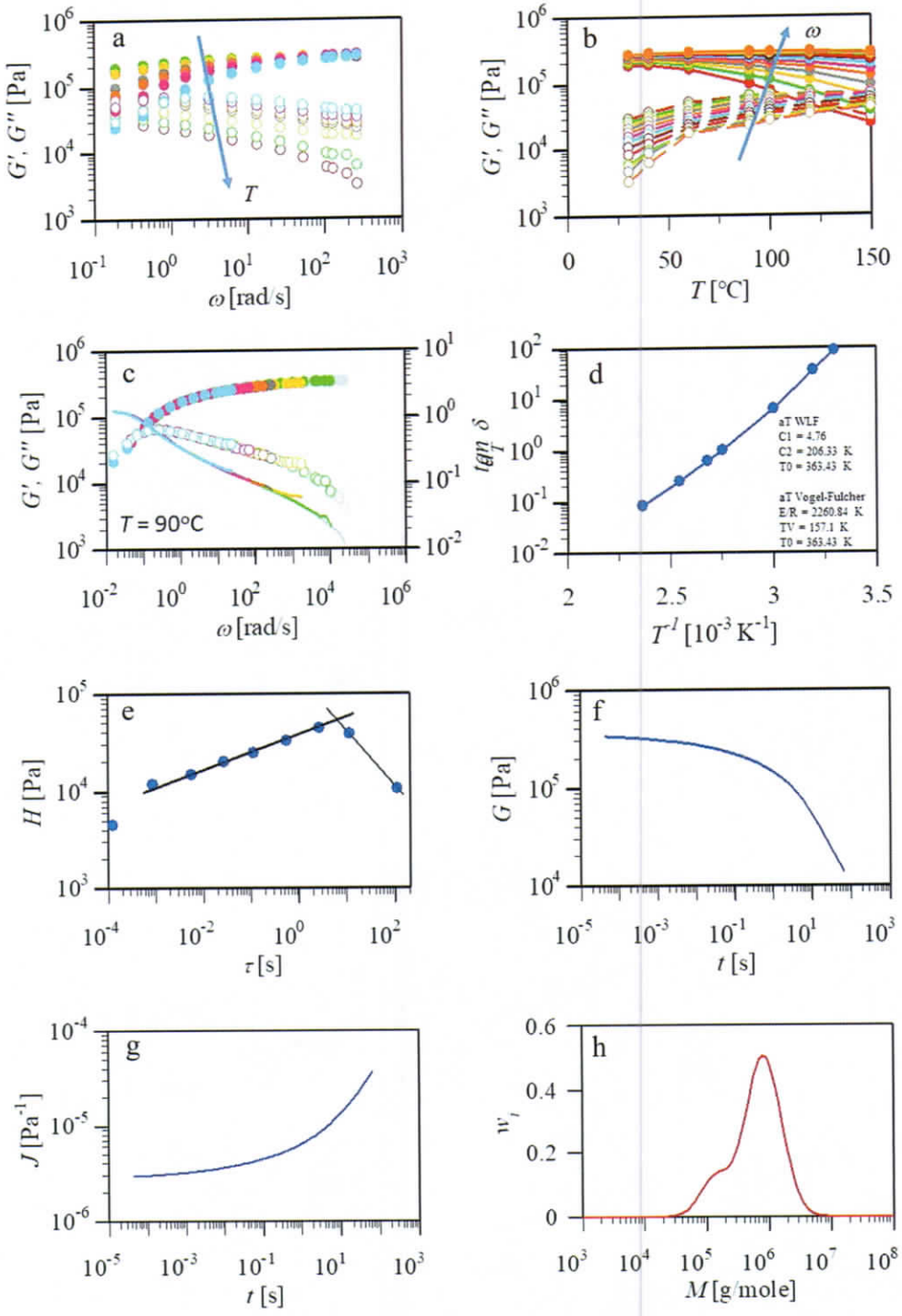

Fig. 1 Dynamic mechanical data of a solution styrene–butadiene rubber. The frequencies were $\omega = 0.19$; 0.44; 0.82; 1.57; 3.14; 6.28; 13.07; 26.33; 52.90; 106.90; 127.70; 193.90; 261.80 rad/s applied at temperatures between 30 °C and 150 °C. The measured dynamic moduli, G' and G'', are the basis for the interactive analysis and plotting. (**a**) The process begins by entering small amplitude oscillatory shear (SAOS) data into IRIS Rheo-Hub and plotting the data; (**b**) the same SAOS data plotted as multi-frequency heating scan; (**c**) the SAOS data get shifted horizontally to a reference temperature $T = 90$ °C; (**d**) the temperature shift factor, belonging to the combined G', G'' of 1c, obeys the WLF format (see fit function plotted and as insert); (**e**) the continuous relaxation time spectrum at $T = 90$ °C gets determined with the parsimonious model of Baumgärtel and Winter; (**f**) from that, the relaxation modulus $G(t)$ derives, belonging to the SAOS data at $T = 90$ °C; (**g**) and the corresponding creep compliance $J(t)$ belonging to SAOS data at $T = 90$ °C; (**h**) the molecular weight distribution as derived from the above SAOS data using the Cocchini/Nobile method

it has been shown that SAOS data support the prediction of the molar mass distribution (Dealy et al. 2018; Thimm et al. 1999). Here, we used the model of Cocchini and Nobile (2003) as implemented in IRIS Rheo-Hub and predict the molar mass distribution of the solution styrene–butadiene rubber sample, Fig. 1h.

The dynamic moduli of Fig. 1a can be combined to express the complex viscosity as shown in Fig. 2. The Cox–Merz format (Cox and Merz 1958), Fig. 2a, often serves as substitute for the steady shear viscosity function $\eta(\dot{\gamma})$, which might be unavailable. This is a useful practice for polymers that have very similar steady shear viscosity function $\eta(\dot{\gamma})$ and complex viscosity $\eta^*(\omega)$. For these polymers, the shape of the curves is fairly identical when substituting frequency ω in $\eta^*(\omega)$ with the shear rate. If the Cox–Merz relation holds, the stress-dependent steady shear viscosity $\eta(\sigma)$ has its counterpart in a complex viscosity $\eta^*(G^*)$ (Winter 2009), Fig. 2b, which helps to magnify temperature effects and sample-to-sample variations in general. A heating scan demonstrates the reduction of the viscosity at elevated temperature, Fig. 2c. The Cox–Merz viscosities were shifted into a master viscosity curve, at 90 °C, Fig. 2d, which is ready to be used at other temperatures within the experimental temperature range. To demonstrate this, the master curve was shifted to 30 °C and 130 °C. Also in Fig. 2d, the 90 °C master curve was expressed as steady shear viscosity $\eta(\sigma)$ in Carreau–Yasuda format (Carreau 1972; Carreau, et al. 1997; Yasuda, et al. 1981), Fig. 2d. The agreement between $\eta(\sigma)$ and $\eta^*(G^*)$ could not be closer. Curve fitting with the Carreau–Yasuda equation provides parameters that are available now for modeling work, for instance.

Example: The Hierarchical Multi-Mode Molecular Stress Function (HMMSF) Model Applied to Filament Stretching

As the rheological properties of the polymers are reflective of their molecular structure, there is an imperative relationship between molecular properties (e.g., architecture, topology, polydispersity, composition) and the flow properties of polymers (Dealy and Larson 2006). Although the modeling of the polymerization reactions and melt forming operations could lead to the prediction of detailed molecular structures of polymers, and thus, to the prediction of the rheological properties, this is in most cases not possible due to the large number of (mostly unknown) polymerization parameters in commercial operations. The HMMSF model (Narimissa and

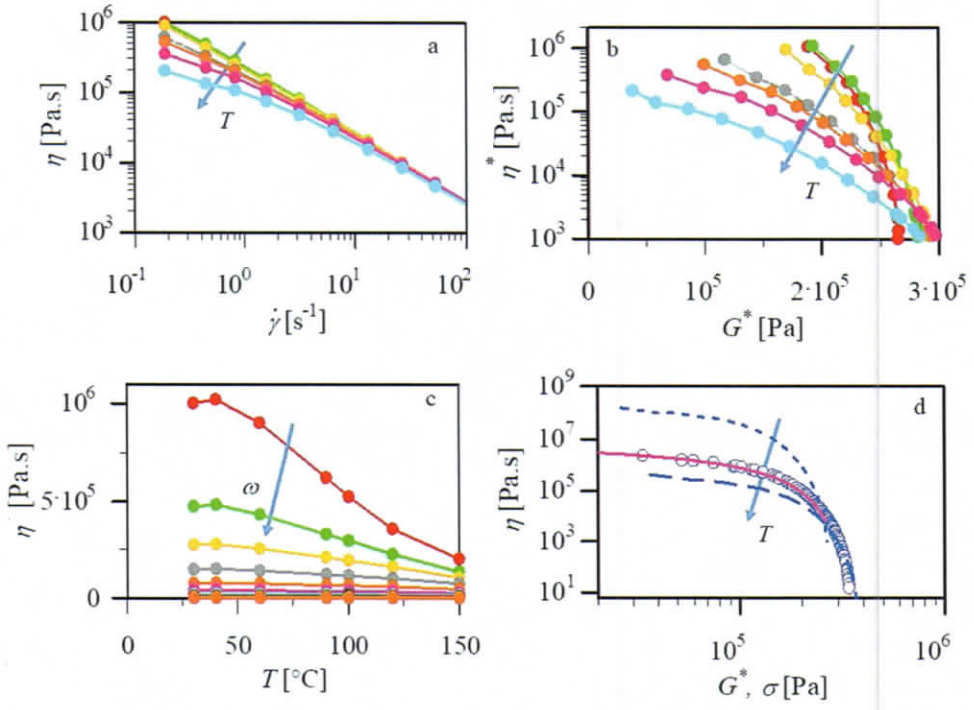

Fig. 2 Complex viscosity as determined from the complex moduli of Fig. 1a. (**a**) Cox–Merz format of the complex viscosity; (**b**) same as 2a, but using the complex modulus G^* as abscissa (instead of frequency ω); (**c**) heating scan of the steady shear viscosity; (**d**) applying time–temperature superposition in preparation of the viscosity master curve at 90 °C. This master curve was shifted to two more temperatures, T-30 °C and T=130 °C. Figure 2d also shows the corresponding steady shear viscosity $\eta(\sigma)$, as expressed with the Carreau–Yasuda function (solid line), superimposed onto the Cox–Merz viscosity $\eta^*(G^*)$ (data points), both at 90 °C. The parameter values in the Carreau–Yasuda function. $\eta(x) = A_1 + \frac{A_0 - A_1}{\left(1+(A_2 x)^{A_4}\right)^{A_3/A_4}}$ are A_0=4.902e+006Pas; A_1=0 Pas; A_2=22.3 s; A_3=0.964; A_4=0.5192, with the shear rate denoted as "x."

Wagner 2016a) recognizes that the rheological effects of complex, and sometimes unknown (e.g., as in long-chain branched systems), molecular structure are already included in the linear viscoelastic relaxation spectrum of the polymer. Therefore, the HMMSF model is based on a few well-defined constitutive assumptions for nonlinear flow, and consequently, it reduces the number of free material parameters to a minimum, i.e., one in extensional flows and two in shear flow. Extensional flow is very sensitive to the macromolecular structure of polymers such as their degree of branching, molecular weight distribution, and cross-linking (Meissner and Hostettler 1994; Narimissa et al. 2014), and this type of deformation is present in almost all processing operations such as blow molding, melt spinning, and biaxial stretching of extruded sheets.

Theoretical Background

The detailed theoretical steps behind the development of the hierarchical multi-mode molecular stress function (HMMSF) model can be found in papers by Narimissa and Wagner for uniaxial and multiaxial extensional flow (Narimissa et al. 2015, 2016; Narimissa and Wagner 2016a, 2016b), for shear flow of polymer melts (Narimissa and Wagner 2016c), and in review articles (Narimissa and Wagner 2018, 2019). We recall that the HMMSF model for both linear and LCB polymer melts is based on the concepts of hierarchical relaxation, dynamic dilution, interchain tube pressure, and convective constraint release.

The extra stress tensor of the hierarchical multi-mode MSF (HMMSF) model is given as

$$\sigma(t) = \sum_i \int_{-\infty}^{t} \frac{\partial G_i(t-t')}{\partial t'} f_i^2(t,t') \mathbf{S}_{DE}^{IA}(t,t') dt' \tag{1}$$

Here, $\mathbf{S}_{DE}^{IA}$ is the Doi and Edwards orientation tensor assuming an independent alignment (IA) of tube segments (Doi and Edwards 1986), which is five times the second-order orientation tensor $\mathbf{S}$,

$$S_{DE}^{IA}(t,t') \equiv 5\langle \frac{u'u'}{u^2} \rangle = 5S(t,t') \tag{2}$$

u' presents the length of the deformed unit vector $\mathbf{u}'$, and the bracket denotes an average over an isotropic distribution of unit vectors at time t', $\mathbf{u}(t')$, which can be expressed as a surface integral over the unit sphere. The molecular stress functions $f_i = f_i(t,t')$ are the inverse of the relative tube diameters a_i of each mode i,

$$f_i(t,t') = a_{i0}/a_i(t,t') \tag{3}$$

$f_i = f_i(t,t')$ is a function of both the observation time t and the time of creation of tube segments by reputation t'. The relaxation modulus $G(t)$ of the melt is represented by discrete Maxwell modes with partial relaxation moduli g_i and relaxation times τ_i taken from the LVE characterization,

$$G(t) = \sum_{j=1}^{n} G_i(t) = \sum_{j=1}^{n} g_j \exp(-t/\tau_j) \tag{4}$$

The mass fraction w_i of dynamically diluted linear or long chain branched (LCB) polymer segments with relaxation time $\tau_i > \tau_D$ is determined by considering the ratio of the relaxation modulus at time $t = \tau_i$ to the dilution modulus $G_D = G(t = \tau_D)$,

$$\begin{aligned} w_i^2 &= \frac{G(t=\tau_i)}{G_D} = \frac{1}{G_D} \sum_{j=1}^{n} g_j \exp(-\tau_i/\tau_j) \quad \text{for } \tau_i > \tau_D \\ w_i^2 &= 1 \qquad\qquad\qquad\qquad\qquad\quad \text{for } \tau_i \le \tau_D \end{aligned} \tag{5}$$

The value of w_i obtained at $t = \tau_i$ is attributed to the chain segments with relaxation time τ_i. Segments with $\tau_i < \tau_D$ are considered to be permanently diluted, i.e., their weight fractions are fixed at $w_i = 1$. Although this may seem to be a very rough estimate, it has been shown to be a sufficiently robust assumption to model the rheology of broadly distributed polymers, largely independent from the number of discrete Maxwell modes used to represent the relaxation modulus $G(t)$ (Narimissa et al. 2015). The evolution equation for the molecular stress function of each mode is expressed as (Narimissa et al. 2015),

$$\frac{\partial f_i}{\partial t} = f_i(\mathbf{K} : \mathbf{S}) - \frac{1}{\alpha}\left(\frac{1}{\tau_i} + \beta CR\right)\left[(f_i - 1)\left(1 - \frac{2}{3}w_i^2\right) + \frac{2}{9}f_i^2(f_i^3 - 1)w_i^2\right] \tag{6}$$

with the initial conditions $f_i(t = t', t) = 1$. The first term on the right hand side represents an on-average affine stretch rate with $\mathbf{K}$ the velocity gradient tensor, the second term takes into account the Rouse relaxation in the longitudinal direction of the tube, and the third term limits molecular stretch due to the interchain tube pressure in the lateral direction of a tube segment (Wagner et al. 2005). The topological parameter α depends on the topology (i.e., chain architecture) of the melt, with

$$\begin{aligned} \alpha &= 1 \text{ for LCB Melts} \\ \alpha &= 1/3 \text{ for polydisperse linear melt} \end{aligned} \tag{7}$$

CR represents a dissipative constraint release (CR) term in shear flow (zero in extensional flow) relating the linear viscoelastic relaxation times τ_i to constraint release relaxation times τ_{iCR} (Ianniruberto and Marrucci 1996; Narimissa and Wagner 2016c),

$$\frac{1}{\tau_{iCR}} = \frac{1}{\tau_i} + \beta\, CR \tag{8}$$

β is the numerical coefficient of the CCR mechanism considered as a fitting parameter; thus, in extensional flow with the constraint release term CR being zero the only fitting parameter is the dilution modulus G_D. The HMMSF model has been proven to be in excellent agreement with experimental data of linear and LCB melts (Narimissa and Wagner 2019), and also it has shown promising results in predicting the crystallization rate and morphology of HDPE (Wingstrand et al. 2017) as well as extensional and shear rheology of low-viscosity polymer melts (Poh et al. 2021a).

Modeling of Extensional and Shear Flows

The interactive capabilities of IRIS become apparent in a combined use of experimental data, shear, and extension, with theoretical predictions superimposed. For demonstration purposes, we chose a high-density polyethylene (HDPE) melt with molar mass 1.24×10^5 g/mol and polydispersity index 9.5 (hereafter PE 124–10) and its recently published rheological data by Morelly and Alvarez (2020) (M&A). This HDPE is supposed to contain a small fraction of short and long-chain branching. The rheological data of the sample are analyzed and combined with predictions of the HMMSF model as implemented in IRIS. Recently, (Poh et al. 2021b) investigated the effects of polydispersity on the elongational deformation of the complete data set of M&A (four commercial HDPEs) by using the HMMSF model via the IRIS software.

Experimental data for this brief demonstration are shown in Fig. 3, all scanned from M&A, digitized, and uploaded into IRIS.

A continuous relaxation time spectrum, $H(\tau)$, was calculated from the storage and loss moduli, G' and G'' of M&A, following the Baumgärtel and Winter (1989) method. The resulting spectrum is shown in Fig. 4a. For the Booij–Palmen plot (1982), Fig. 4b, the loss angle (δ) was calculated as a function of the complex modulus G^* using the continuous relaxation time spectrum and overlaid with the experimental data of M&A extracted from storage and loss moduli (Fig. 3a). The overlay provides a visual check of the IRIS-calculated relaxation time spectrum.

The IRIS software provides extensional modeling with a choice of theories. Here, the HMMSF model was selected and activated in the IRIS satellite section of *Non-Linear Viscoelastic Theory* tab and under *Melts and Solutions*. We recall that the HMMSF model can be used to model linear and LCB melts in uniaxial and multiaxial extensional flow as well as shear flow of polymer melts. This will be demonstrated in the next few figures for PE-124–10. While short-chain branching is expected to affect only the dilution modulus, long-chain branching leads to an enhanced slope of the elongational stress growth coefficient. As the HDPE sample contains a small fraction of long-chain branching, in a first attempt the LCB version of the HMMSF model (see Eq. 7) was used to predict the transient elongational

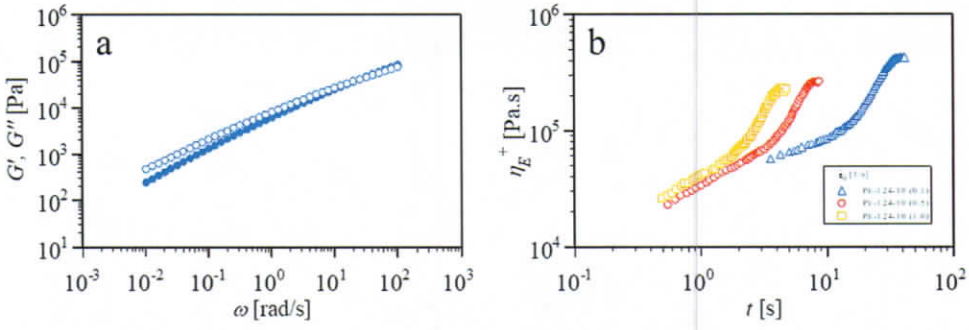

Fig. 3 The experimental data used in this IRIS demonstration are those of high-density polyethylene PE-124–10. The data were scanned from a publication of Morelly and Alvarez (2020) and inserted into IRIS Rheo-Hub. The scanned data are (**a**) dynamic moduli G' and G'', and (**b**) transient elongational viscosity from filament stretching rheometry

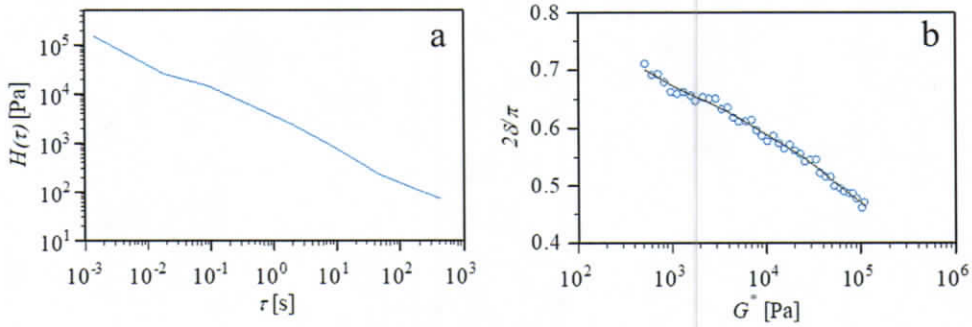

Fig. 4 **a** Continuous relaxation time spectrum calculated from G' and G'' data (Fig. 3a) with the method of Baumgärtel and Winter (1989). **b** Visual consistency check: Booij–Palmen plot (Booij and Palmen 1982) as overlay of the δ-G^* prediction (line) from the continuous spectrum, $H(\tau)$,and the scanned G'G'' data of Fig. 3a converted to $G^*(\delta)$ (symbols)

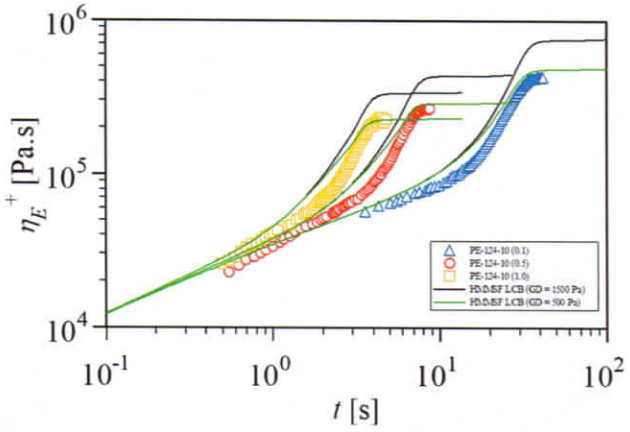

Fig. 5 Comparison between data (symbols) of the elongational stress growth coefficient of PE 124–10 at 160 °C from M&A with predictions (continuous lines) of the HMMSF LCB model with dilution modulus $G_{D\,=}$ 500 and 1500 Pa. The dashed line marks the linear viscoelastic limit as calculated with $H(\tau)$

viscosity. Figure 5 shows that the predictions of the HMMSF LCB model with $G_D = 500$ and 1500 Pa do not fit the extensional stress growth coefficient at all experimental strain rates investigated (0.1, 0.5, and 1.0 s^{-1}). The slope of the stress growth predicted is significantly more enhanced than observed experimentally.

In Fig. 6, the linear version of the HMMSF model according to Eq. (7) was used to predict the elongational deformation with dilution modulus $G_D = 1700$ Pa for all three strain rates (0.1, 0.5 and 1.0 s^{-1}), and excellent agreement between data and model is achieved for stress growth coefficient as well as steady-state elongational viscosity. To demonstrate the sensitivity of the HMMSF model predictions with

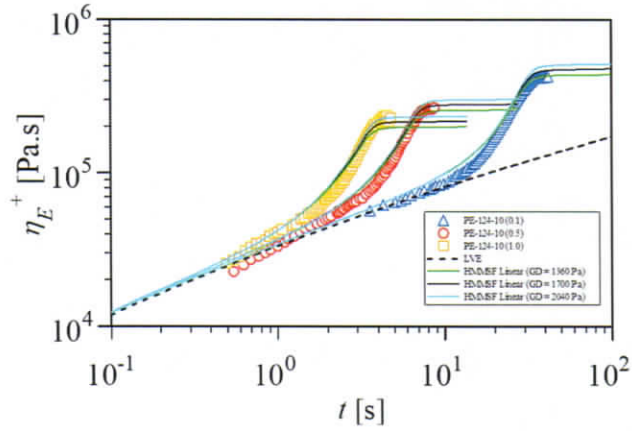

Fig. 6 Comparison between data (symbols) of the elongational stress growth coefficient of PE 124–10 at 160 °C from M&A with predictions (continuous lines) of the HMMSF linear model with dilution modulus $G_{D\,=}$ 1360, 1700, and 2040 Pa. The dashed line marks the linear viscoelastic limit as calculated with $H(\tau)$

respect to the value of the dilution modulus, G_D was varied by plus/minus 20% from the optimal value of 1700 Pa. Both $G_D = 1360$ and 2040 Pa show either overpredictions in the lower strain rates or underprediction in the higher strain rates (Fig. 6). The linear viscoelastic envelope curve can be added to the plot by choosing a rate as low as 10^{-5} s^{-1}.

Figures 5 and 6 demonstrate that the small fraction of long-chain branched chains in this HDPE is most likely consisting of asymmetric stars, i.e., basically linear chains with only one branch point. It is well known that stars behave like linear polymers in extensional flow (Ianniruberto and Marrucci 2012). Huang et al. (2016) measured the extensional rheology of three PS melts with linear, 3-arm asymmetric star, and 3-arm symmetric star architectures and found that their rheological behavior in extensional flow is identical when stretched faster than the inverse Rouse time. In sufficiently fast extensional flows, the star molecules are highly aligned and thus have a similar conformation as the linear molecules.

In addition to the excellent agreement of the start-up of the elongational viscosity data and model, the comparison of data and model demonstrates two important features: (1) LVE as determined from SAOS and the linear viscoelastic extensional start-up viscosity agree within experimental accuracy, confirming the consistency of different measurement methods and rheometers; (2) The traces of LCB branching in this HDPE are most likely asymmetric stars, i.e., basically linear chains with only one branch point. The comparison of data and model reveals therefore surprising new features which might warrant further investigation.

While extensional polymer characterization is mostly conducted in uniaxial extensional flow, planar extensional deformation is of great significance in polymer processing as it dominates free surface extensional flow in the vicinity of dies, where one dimension is restricted. Planar extension is characterized by two viscosity functions, one in the direction of flow (η_{P1}), and one in the cross-direction of flow (η_{P2}). Other polymer processes such as e.g. bubble growth in foaming rely on biaxial extension characterized by the equibiaxial viscosity η_B. The HMMSF satellite of IRIS allows predicting these viscosity functions based exclusively on SAOS data and the characterization in uniaxial extensional flow, i.e. the dilution modulus G_D. Figure 7 demonstrates the use of the HMMSF model in the predictions of stress growth coefficients of PE 124–10 at 160 °C for planar and equibiaxial extensional flows with dilution modulus $G_D = 1700$ Pa.

To demonstrate shear flow predictions of the HMMSF model, the complex viscosity data of PE 124–10 calculated from the G' and G'' data were used to determine the shear parameter β of the HMMSF model (Fig. 8). For $\beta = 1.84$

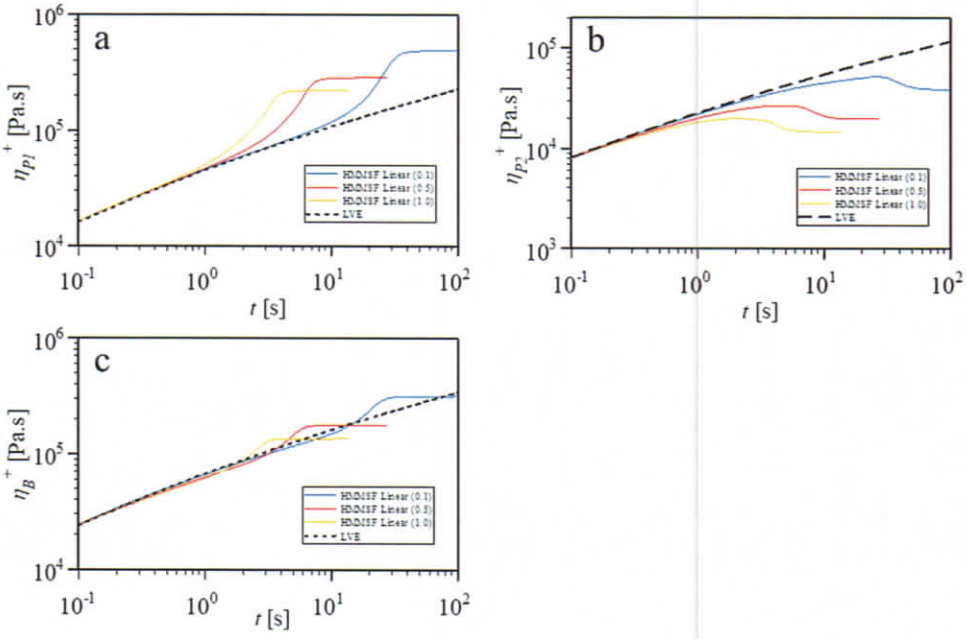

Fig. 7 Extensional stress growth coefficient predictions (continuous lines) of PE 124–10 at 160 °C from M&A with the HMMSF linear model for planar viscosity in (**a**) flow direction, (**b**) cross-flow direction, and (**c**) equibiaxial viscosity. The dashed lines mark the linear viscoelastic limits as calculated from $H(\tau)$

optimal agreement was achieved between complex viscosity data and steady-state shear viscosity predictions of the HMMSF linear model with dilution modulus of $G_D = 1700$ Pa. Predictions for strain rates of 0.01, 0.05, 0.1, 0.5, 1.0, 5.0, 10.0, 50.0, and 100.0 s^{-1} are fitted in Fig. 8 by the Cross model (Cross 1979) implemented in IRIS. Figure 9 shows the predictions for transient shear viscosity and first normal stress function of PE 124–10 with $G_D = 1700$ Pa and $\beta = 1.84$ for strain rates of 0.01, 0.05, 0.1, 0.5, 1.0, 5.0, and 10.0 s^{-1}. Thus, based on the LVE characterization and only two nonlinear material parameters, G_D and β, the HMMSF model predicts the flow behavior of PE 124–10 across all deformation modes, from uniaxial flow to planar, biaxial, and shear flow.

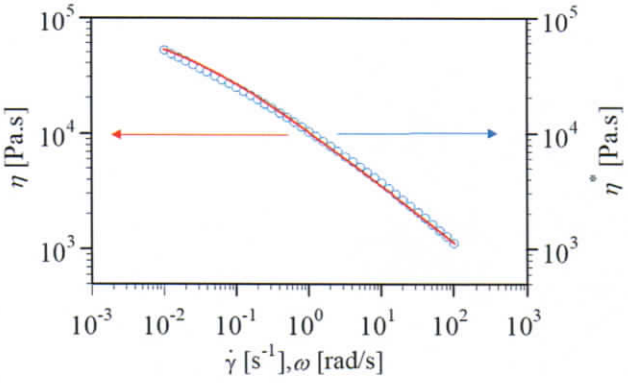

Fig. 8 Comparison between complex viscosity data, $\eta*(\omega)$, (open symbols) calculated from G' and G'' data of PE 124–10 with steady-state shear viscosity predictions, $\eta(\dot{\gamma})$, (continuous line) of the HMMSF linear model with $G_D = 1700$ Pa and $\beta = 1.84$ fitted by the Cross model

Conclusions

As demonstrated in the examples above, much insight can be gained by bringing rheological experiments and theories together in quantitative ways. Such merging became possible through the interactive IRIS program with its linear viscoelastic analysis tools, motivated by the Boltzmann theory, and its nonlinear viscoelasticity theory satellite codes. The IRIS software utilizes reliable principles and methods and, in this way, creates an environment in which trustworthy results are generated almost instantly. Rheological experiments can be evaluated instantly, even before samples are taken from the rheometer (Winter 1997), and compared to theoretical predictions. The results are expressed in rheological visuals for dissemination beyond the rheology laboratory. IRIS's standardized data format allows efficient data sharing and retrieval as needed, even remotely. Typically, this efficient and visually comprehensive approach to rheology reveals dynamic patters of specific materials—for example, the relaxation of long linear flexible polymers (Baumgärtel et al. 1990) and colloids undergoing glass transition (Siebenbürger et al. 2009; Winter 2013). The IRIS methodologies have been tried and tested extensively. Even then, we keep adding more and/or better satellite codes to the IRIS platform.

Rheological data are rich with valuable information. A deeper analysis helps us to recognize what the data entails. IRIS facilitates such deeper analysis as demonstrated here by the two examples presented. Over the past quarter century,

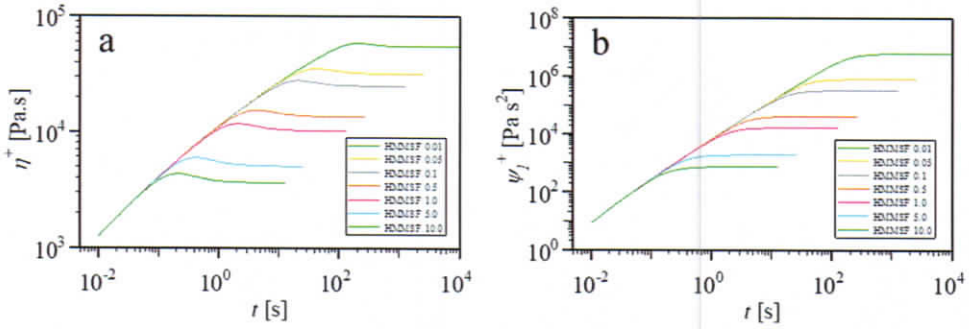

Fig. 9 Predictions (lines) of (**a**) shear viscosity and (**b**) first normal stress function of PE 124–10 at 160 °C using the HMMSF linear model with $G_D = 1700$ Pa and $\beta = 1.84$ for strain rates of 0.01, 0.05, 0.1, 0.5, 1.0, 5.0, and 10.0 s^{-1}

IRIS has proven invaluable in revealing and exploring the rheological secrets of soft matter.

Supplementary Information The online version contains supplementary material available at https://doi.org/10.1007/s00397-022-01331-6.

Acknowledgements We thank Synthos for the provision of SAOS results and the permission to use these in a demonstration of IRIS "at work." Greatly acknowledged are the contributions of many rheologists who provided their codes for implementation in IRIS. IRIS has permission to interface these codes so that data can be transferred across codes and results can be overlaid in specialized graphical displays. Decisions about possible access to the individual original codes remain by the authors of these original codes. The use of IRIS requires an activation code. HHW acknowledges the financial support of the Petroleum Research Fund, PRF# 58675-ND10. LP and EN acknowledge the financial support from the Ministry of Science and Technology of China, MOST Grant # QN2021030003L.

References

Baumgärtel M, Schausberger A, Winter HH (1990) The relaxation of polymers with linear flexible chains of uniform length. Rheol Acta 29:400–408

Baumgärtel M, Winter HH (1989) Determination of discrete relaxation and retardation time spectra from dynamic mechanical data. Rheol Acta 28:511–519

Baumgärtel M, Winter HH (1992) Interrelation between continuous and discrete relaxation time spectra. J Nonnewton Fluid Mech 44:15–36

Blackwell RJ, Harlen OG, McLeish TCB (2001) Theoretical linear and nonlinear rheology of symmetric treelike polymer melts. Macromolecules 34:2579–2596 (Export Date 24 August 2013)

Booij HC, Palmen JHM (1982) Some aspects of linear and nonlinear viscoelastic behaviour of polymer melts in shear. Rheol Acta 21:376–387. https://doi.org/10.1007/BF01534297

Carreau PJ (1972) Rheological Equations from Molecular Network Theories. Trans Soc Rheol 16:99–127. https://doi.org/10.1122/1.549276

Carreau PJ, De Kee DCR, Chhabra RP (1997) Rheology of Polymeric Systems. Hanser Publishers, New York

Cocchini F, Nobile M (2003) Constrained inversion of rheological data to molecular weight distribution for polymer melts. Rheol Acta 42:232–242. https://doi.org/10.1007/s00397-002-0273-8

Colby RH (1989) Breakdown of time-temperature superposition in miscible polymer blends. Polymer 30:1275–1278. https://doi.org/10.1016/0032-3861(89)90048-7

Cox WP, Merz EH (1958) Correlation of dynamic and steady flow viscosities. J Polym Sci 28:619–622. https://doi.org/10.1002/pol.1958.1202811812

Cross MM (1979) Relation between viscoelasticity and shear-thinning behaviour in liquids. Rheol Acta 18:609–614. https://doi.org/10.1007/BF01520357

Dealy JM (1995) Official nomenclature for material functions describing the response of a viscoelastic fluid to various shearing and extensional deformations. J Rheol 39:253–265. https://doi.org/10.1122/1.4765670

Dealy JM, Larson RG (2006) Structure and Rheology of Molten Polymers - From Structure to Flow Behavior and Back Again. Hanser Publishers, Munich

Dealy JM, Read DJ, Larson RG (2018) Structure and rheology of molten polymers: from structure to flow behavior and back again. Hanser Publishers, Munich

Doi M, Edwards SF (1978) Dynamics of concentrated polymer systems. Part 3. - The constitutive equation. J Chem Soc Faraday Trans 2 Mol Chem Phys 74:1818–1832

Doi M, Edwards SF (1986) The Theory of Polymer Dynamics. Oxford University Press, Oxford

Ewoldt RH, Hosoi AE, McKinley GH (2008) New measures for characterizing nonlinear viscoelasticity in large amplitude oscillatory shear. J Rheol 52:1427–1458. https://doi.org/10.1122/1.2970095

Ferry JD (1980) Viscoelastic Properties of Polymers. John Wiley and Sons, New York

Fuchs M, Ballauff M (2005a) Flow curves of dense colloidal dispersions: Schematic model analysis of the shear-dependent viscosity near the colloidal glass transition. J Chem Phys 122:094707. https://doi.org/10.1063/1.1859285

Fuchs M, Ballauff M (2005b) Nonlinear rheology of dense colloidal dispersions: A phenomenological model and its connection to mode coupling theory. Colloids Surf A Physicochem Eng Asp 270–271:232–238. https://doi.org/10.1016/j.colsurfa.2005.06.017

Fuchs M, Cates ME (2002a) Non-Newtonian viscosity of interacting Brownian particles: comparison of theory and data. J Phys: Condens Matter 15:S401–S406. https://doi.org/10.1088/0953-8984/15/1/355

Fuchs M, Cates ME (2002b) Theory of Nonlinear Rheology and Yielding of Dense Colloidal Suspensions. Phys Rev Lett 89:248304. https://doi.org/10.1103/PhysRevLett.89.248304

Huang Q, Agostini S, Hengeller L, Shivokhin M, Alvarez NJ, Hutchings LR, Hassager O (2016) Dynamics of star polymers in fast extensional flow and stress relaxation. Macromolecules 49:6694–6699

Ianniruberto G, Marrucci G (1996) On compatibility of the Cox-Merz rule with the model of Doi and Edwards. J Non-Newtonian Fluid Mech 65:241–246. https://doi.org/10.1016/0377-0257(96)01433-4

Ianniruberto G, Marrucci G (2012) Entangled melts of branched PS behave like linear PS in the steady state of fast elongational flows. Macromolecules 46:267–275

Larson R (2001) Combinatorial rheology of branched polymer melts. Macromolecules 34:4556–4571

Laukkanen OV, Winter HH (2018) The dynamic fragility and apparent activation energy of bitumens as expressed by a modified Kaelble equation. J Non-Cryst Solids 499:289–299

Liu Y, Momani B, Winter HH, Perry SL (2017) Rheological characterization of liquid-to-solid transitions in bulk polyelectrolyte complexes. Soft Matter 13:7332–7340

Lodge AS (1956) A network theory of flow birefringence and stress in concentrated polymer solutions. Trans Faraday Soc 52:120–130. https://doi.org/10.1039/TF9565200120

Masubuchi Y, Ianniruberto G, Greco F, Marrucci G (2003) Entanglement molecular weight and frequency response of sliplink networks. J Chem Phys 119:6925–6930

Masubuchi Y, Ianniruberto G, Greco F, Marrucci G (2004) Molecular simulations of the long-time behaviour of entangled polymeric liquids by the primitive chain network model. Modell Simul Mater Sci Eng 12:S91–S100. https://doi.org/10.1088/0965-0393/12/3/s03

Masubuchi Y, Takimoto J-I, Koyama K, Ianniruberto G, Marrucci G, Greco F (2001) Brownian simulations of a network of reptating primitive chains. J Chem Phys 115:4387–4394

Maxwell JC (1867) IV. On the dynamical theory of gases. Philos Trans R Soc Lond 157:49–88. https://doi.org/10.1098/rstl.1867.0004

McLeish TCB, Allgaier J, Bick DK, Bishko G, Biswas P, Blackwell R, Blottière B, Clarke N, Gibbs B, Groves DJ, Hakiki A, Heenan RK, Johnson JM, Kant R, Read DJ, Young RN (1999) Dynamics of entangled H-polymers: Theory, rheology, and neutron-scattering. Macromolecules 32:6734–6758 (DOI Export Date 24 August 2013)

McLeish TCB, Larson RG (1998) Molecular constitutive equations for a class of branched polymers: The pom-pom polymer. J Rheol 42:81–110. https://doi.org/10.1122/1.550933

Meissner J, Hostettler J (1994) A new elongational rheometer for polymer melts and other highly viscoelastic liquids. Rheol Acta 33:1–21. https://doi.org/10.1007/BF00453459

Milner ST, McLeish TCB (1997) Parameter-Free Theory for Stress Relaxation in Star Polymer Melts. Macromolecules 30:2159–2166. https://doi.org/10.1021/ma961559f

Milner ST, McLeish TCB (1998) Reptation and contour-length fluctuations in melts of linear polymers. Phys Rev Lett 81:725

Morelly SL, Alvarez NJ (2020) Characterizing long-chain branching in commercial HDPE samples via linear viscoelasticity and extensional rheology. Rheol Acta 59:797–807. https://doi.org/10.1007/s00397-020-01233-5

Mours M, Winter HH (1994) Time-resolved rheometry. Rheol Acta 33:385–397

Narimissa E, Gupta RK, Kao N, Nguyen DA, Bhattacharya SN (2014) Extensional Rheological Investigation of Biodegradable Polylactide-Nanographite Platelet Composites via Constitutive Equation Modeling. Macromol Mater Eng 299:851–868. https://doi.org/10.1002/mame.201300382

Narimissa E, Rolón-Garrido VH, Wagner MH (2015) A Hierarchical Multi-Mode MSF Model for Long-Chain Branched Polymer Melts Part I: Elongational Flow. Rheol Acta 54:779–791. https://doi.org/10.1007/s00397-015-0879-2

Narimissa E, Rolón-Garrido VH, Wagner MH (2016) A hierarchical multi-mode MSF model for long-chain branched polymer melts part II: multiaxial extensional flows. Rheol Acta 55:327–333. https://doi.org/10.1007/s00397-016-0922-y

Narimissa E, Wagner MH (2016a) From Linear Viscoelasticity to Elongational Flow of Polydisperse Polymer Melts: the Hierarchical Multi-mode Molecular Stress Function Model. Polymer. https://doi.org/10.1016/j.polymer.2016.06.005

Narimissa E, Wagner MH (2016b) A Hierarchical Multi-Mode Molecular Stress Function Model for Linear Polymer Melts in Extensional Flows. J Rheol 60:625–636. https://doi.org/10.1122/1.4953442

Narimissa E, Wagner MH (2016c) A Hierarchical Multi-Mode MSF Model for Long-Chain Branched Polymer Melts Part III: Shear Flow. Rheol Acta 55:633–639. https://doi.org/10.1007/s00397-016-0939-2

Narimissa E, Wagner MH (2018) Review of the hierarchical multi-mode molecular stress function model for broadly distributed linear and LCB polymer melts. Poly Eng & Sci 59:573–583. https://doi.org/10.1002/pen.24972

Narimissa E, Wagner MH (2019) Review on tube model based constitutive equations for polydisperse linear and long-chain branched polymer melts. J Rheol 63:361–375. https://doi.org/10.1122/1.5064642

Nobile MR, Cocchini F (2001) Evaluation of molecular weight distribution from dynamic moduli. Rheol Acta 40:111–119. https://doi.org/10.1007/s003970000141

Palierne JF, Lequeux F (1991) Sausage instability of a thread in a matrix; linear theory for viscoelastic fluids and interface. J Non-newton Fluid Mech 40:289–306. https://doi.org/10.1016/0377-0257(91)87014-O

Park SJ, Larson RG (2004) Tube Dilation and Reptation in Binary Blends of Monodisperse Linear Polymers. Macromolecules 37:597–604. https://doi.org/10.1021/ma0343683

Park SJ, Larson RG (2005) Modeling the linear viscoelastic properties of metallocene-catalyzed high density polyethylenes with long-chain branching. J Rheol 49:523–536. https://doi.org/10.1122/1.1853382

Poh L, Li B, Yu W, Narimissa E, Wagner MH (2021a) Modeling of nonlinear extensional and shear rheology of low-viscosity polymer melts. Polym Eng Sci 61:1077–1086. https://doi.org/10.1002/pen.25637

Poh L, Narimissa E, Wagner MH (2021b) Modelling of Elongational Flow of HDPE Melts by Hierarchical Multi-Mode Molecular Stress Function Model. Polymers 13:3217. https://doi.org/10.3390/polym13193217

Pryke A, Blackwell RJ, McLeish TCB, Young RN (2002) Synthesis, Hydrogenation, and Rheology of 1,2-Polybutadiene Star Polymers. Macromolecules 35:467–472. https://doi.org/10.1021/ma010350l

Rouse PE (1953) A Theory of the Linear Viscoelastic Properties of Dilute Solutions of Coiling Polymers. J Chem Phys 21:1272–1280. https://doi.org/10.1063/1.1699180

Rowe GM, Sharrock MJ (2011) Alternate shift factor relationship for describing temperature dependency of viscoelastic behavior of asphalt materials. Transp Res Rec J Transp Res Board 2207:125–135

Siebenbürger M, Fuchs M, Winter H, Ballauff M (2009) Viscoelasticity and shear flow of concentrated, noncrystallizing colloidal suspensions: Comparison with mode-coupling theory. J Rheol 53:707–726. https://doi.org/10.1122/1.3093088

Stephens TS, Winter HH, Gottlieb M (1988) The steady shear viscosity of filled polymeric liquids described by a linear superposition of two relaxation mechanisms. Rheol Acta 27:263–272. https://doi.org/10.1007/BF01329742

Thien NP, Tanner RI (1977) A new constitutive equation derived from network theory. J Non-Newtonian Fluid Mech 2:353–365

Thimm W, Friedrich C, Honerkamp J (1999) Determination of Molecular Weight Distributions from Rheological Data: An Application to Polystyrene, Polymethylmethacrylate and Isotactic Polypropylene. Applied Rheology 9:150–157. https://doi.org/10.1515/arh-2009-0010

Voigtmann T, Puertas AM, Fuchs M (2004) Tagged-particle dynamics in a hard-sphere system: Mode-coupling theory analysis. Phys Rev E 70:061506. https://doi.org/10.1103/PhysRevE.70.061506

Wagner MH, Kheirandish S, Hassager O (2005) Quantitative prediction of transient and steady-state elongational viscosity of nearly monodisperse polystyrene melts. J Rheol 49:1317–1327. https://doi.org/10.1122/1.2048741

Wagner MH, Rubio P, Bastian H (2001) The molecular stress function model for polydisperse polymer melts with dissipative convective constraint release. J Rheology 45:1387–1412. https://doi.org/10.1122/1.1413503

Wagner MH, Yamaguchi M, Takahashi M (2003) Quantitative assessment of strain hardening of low-density polyethylene melts by the molecular stress function model. J Rheol 47:779–793. https://doi.org/10.1122/1.1562155

Williams ML, Landel RF, Ferry JD (1955) The temperature dependence of relaxation mechanisms in amorphous polymers and other glass-forming liquids. J Am Chem Soc 77:3701–3707

Wingstrand SL, Shen B, Kornfield JA, Mortensen K, Parisi D, Vlassopoulos D, Hassager O (2017) Rheological Link Between Polymer Melts with a High Molecular Weight Tail and Enhanced Formation of Shish-Kebabs. ACS Macro Lett 6:1268–1273

Winter HH (1997) Analysis of dynamic mechanical data: inversion into a relaxation time spectrum and consistency check. J Nonnewton Fluid Mech 68:225–239. https://doi.org/10.1016/S0377-0257(96)01512-1

Winter HH (2009) Three views of viscoelasticity for Cox-Merz materials. Rheol Acta 48:241–243. https://doi.org/10.1007/s00397-008-0329-5

Winter HH (2013) Glass Transition as the Rheological Inverse of Gelation. Macromolecules 46:2425–2432. https://doi.org/10.1021/ma400086v

Winter HH, Chambon F (1986) Analysis of Linear Viscoelasticity of a Crosslinking Polymer at the Gel Point. J Rheol 30:367–382

Winter HH, Mours M (2006) The cyber infrastructure initiative for rheology. Rheol Acta 45:331–338

Yasuda K, Armstrong RC, Cohen RE (1981) Shear flow properties of concentrated solutions of linear and star branched polystyrenes. Rheol Acta 20:163–178. https://doi.org/10.1007/BF01513059

Yavitt BM, Fei H-F, Kopanati GN, Winter HH, Watkins JJ (2019) Power Law Relaxations in Lamellae Forming Brush Block Copolymers with Asymmetric Molecular Shape. Macromolecules 52:1557–1566. https://doi.org/10.1021/acs.macromol.8b01843

Zimm BH (1956) Dynamics of Polymer Molecules in Dilute Solution: Viscoelasticity, Flow Birefringence and Dielectric Loss. J Chem Phys 24:269–278. https://doi.org/10.1063/1.1742462

SUPPLEMENT to:

Poh L, Narimissa E, Wagner, Winter HH Interactive Shear and Extensional Rheology—25 years of IRIS Software. *Rheol Acta* (2022). https://doi.org/10.1007/s00397-022-01331-

Linear Viscoelastic Data Analysis and Modelling of a Polystyrene

The analysis of example 1 (main paper) is applicable in general, not just to the solution styrene-butadiene rubber of the main paper. This is demonstrated here by repeating the linear viscoelastic analysis with another polymer: a commercial polystyrene (PS) represented by dynamic moduli, *G*' and *G*'', as measured in SAOS frequency scans at seven temperatures, Figure S1a. Higher temperatures resulted in lower *G*', *G*'' for the PS, which becomes more visible in the multi-frequency heating scan, Figure S1b. Horizontal shifting combines the entire data set into master curves, here at a reference temperature of T=205°C, Figure S1c. By applying time-temperature shift to this polymer, the experimental frequency window is significantly broadened. The horizontal shift factor, a_T, follows the well-known WLF format (Ferry 1980), Figure S1d. The continuous spectrum, $H(\tau)$, Figure S1e, calculated with the parsimonious model (Baumgärtel and Winter 1989, 1992), allows calculation of many more material functions (Ferry (1980) , such as the relaxation modulus $G(t)$ and the creep compliance $J(t)$, Figures S1f and g. For linear polymers, it has been shown that SAOS data allow the prediction of the molar mass distribution (Dealy, et al. 2018, Thimm, et al. 1999). Here we used the model of Cocchini and Nobile (2003) as implemented in IRIS Rheo-Hub and predict the molar mass distribution of the PS sample, Figure S1h.

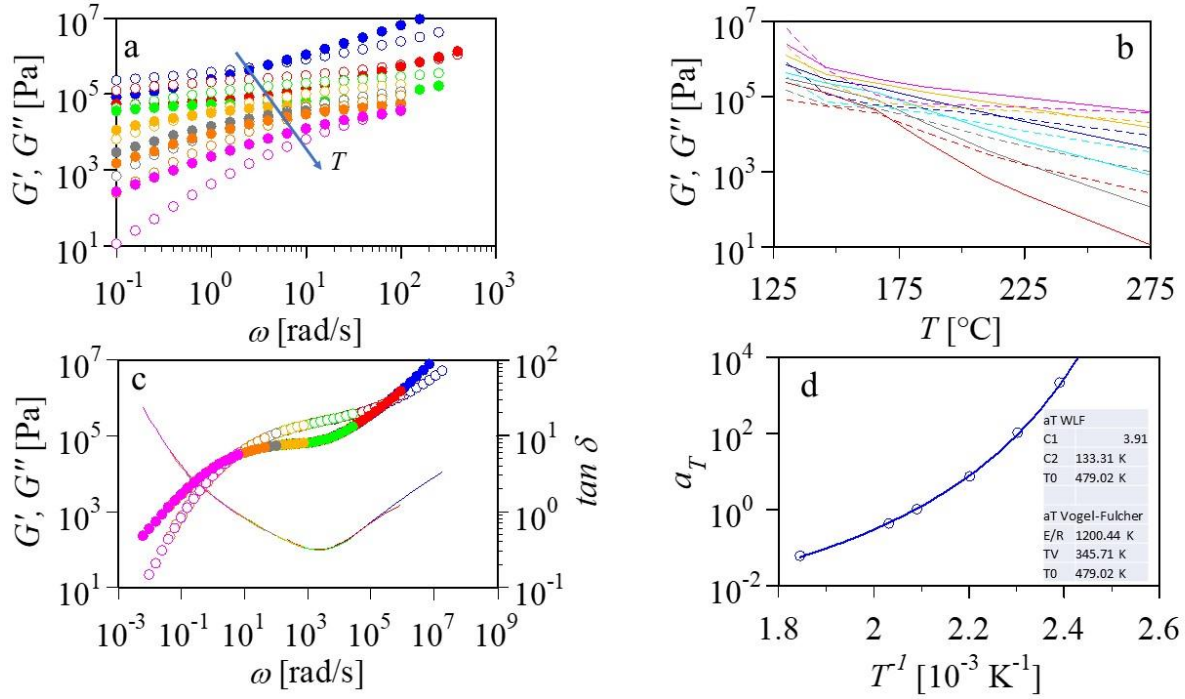

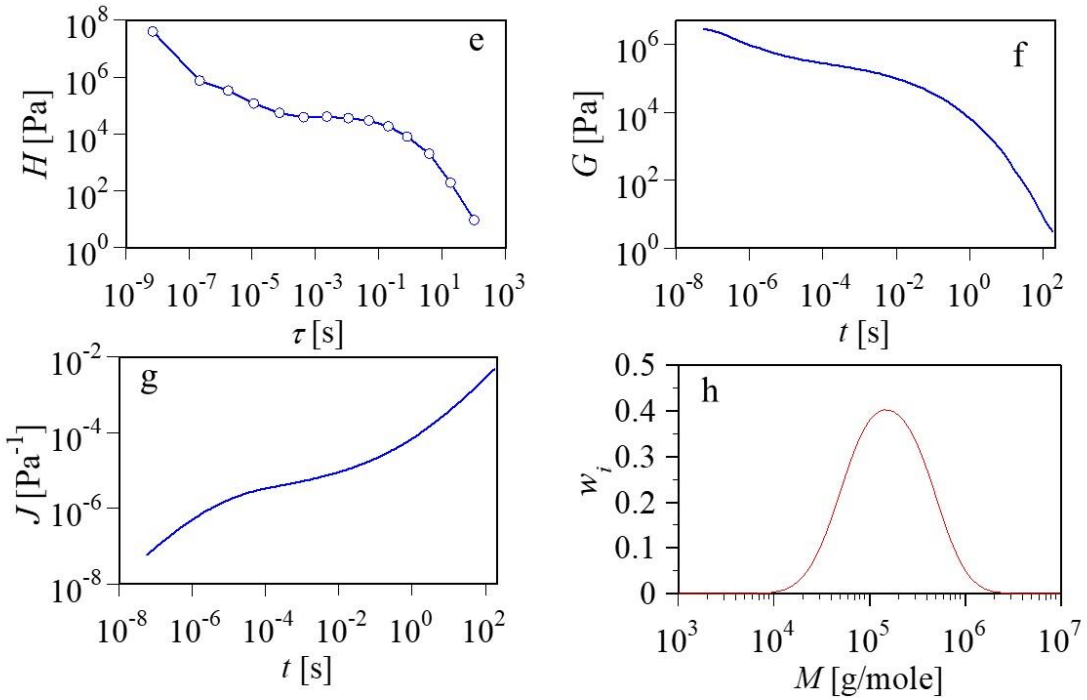

Figure S1: Dynamic mechanical data of a commercial polystyrene (PS). The frequencies range from ω=0.1 to above 100 rad/s at temperatures between 132ºC and 269ºC. The measured dynamic moduli, G' and G'', were entered into IRIS Rheo-Hub and analyzed using the interactive IRIS analysis and plotting: (a) small amplitude oscillatory shear (SAOS) data input from experiment; (b) the same SAOS data plotted as multi-frequency heating scan; (c) the SAOS data get shifted horizontally to a reference temperature T=205ºC; (d) the temperature shift factor belonging to the combined G', G'' of 1c, obeys the WLF format (see fit function plotted and as insert); (e) the continuous relaxation time spectrum at T=205 ºC gets determined with the parsimonious model of Baumgärtel and Winter; (f) from that, the relaxation modulus $G(t)$ derives, belonging to the SAOS data at T=205 ºC; (g) and the corresponding creep compliance $J(t)$ belonging to SAOS data at T=205ºC; (h) the molecular weight distribution as derived from the above SAOS data using the Cocchini/Nobile Method.

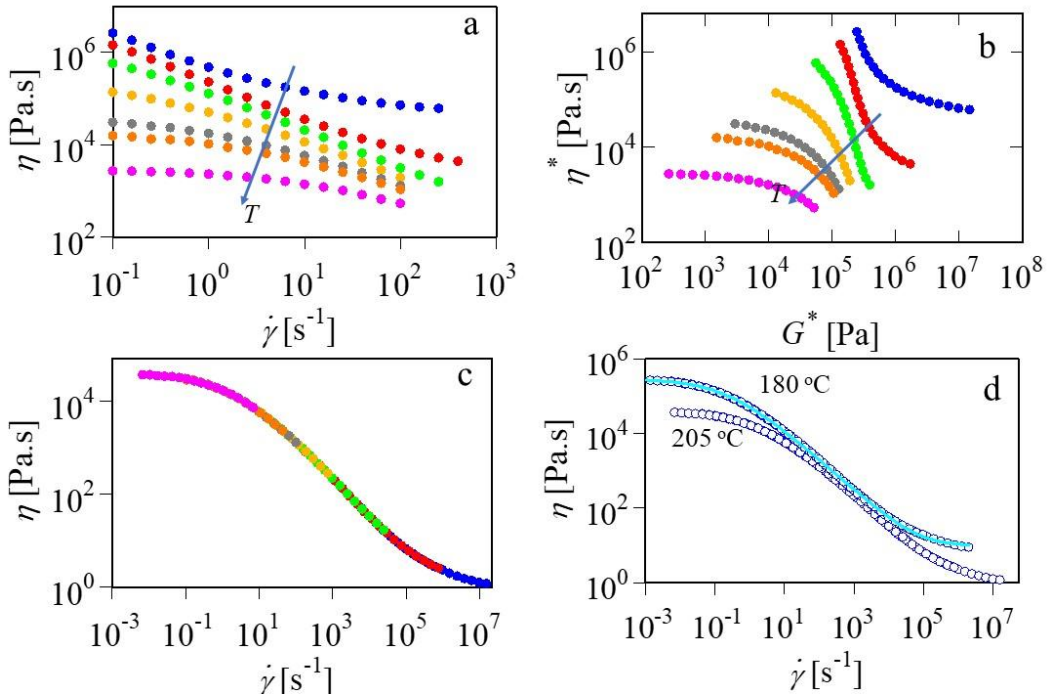

Figure S2: Complex viscosity as determined from the complex moduli of Figure S1a. (a) Cox-Merz format of the complex viscosity; (b) same as 2a, but using the complex modulus G^* as abscissa (instead of frequency ω); (c) applying time-temperature superposition in preparation of the viscosity master curve at 205°C. The master curve has been shifted to a new temperature, which is chosen here as 180 °C. The so derived viscosity can be expressed with the Carreau-Yasuda function (line drawn through the 180 °C data in Figure S2d). The parameter values in the Carreau-Yasuda function

$$\eta(x) = A_1 + \frac{A_0 - A_1}{\left(1 + (A_2 x)^{A_4}\right)^{A_3/A_4}}$$

are A_0=3.90 Pas; A_1=1.31Pas; A_2=5.52s; A_3=0.82; A_4=0.54, with the shear rate denoted as "x".

The dynamic moduli of Figure S1a can be combined to express the complex viscosity as shown in Figure S2. The Cox-Merz format (Cox and Merz 1958), Figure S2a, often serves as substitute for the steady shear viscosity function $\eta(\dot{\gamma})$. The steady shear viscosity $\eta(\sigma)$ has its counterpart in a complex viscosity $\eta^*(G*)$ (Winter 2009), Figure S2b. The Cox-Merz viscosities were shifted into a master viscosity curve, again at 205 °C, Figure S2c, which is ready to be used at other temperatures within the experimental temperature range. To demonstrate this, the master curve was shifted to 180 °C and expressed in Carreau-Yasuda format, Figure S2d,

Filament Stretching data of additional M&A polymers were published by Poh et al. (2021a). Tabulated relaxation time spectra can be found there also. The spectra published by M&A were replaced by the parsimonious model (Baumgärtel and Winter, 1989) so that the experimental data could be expressed more closely.

References: same as in main paper